

Short Communication

Preparation of new composite electrolytes for solid-state lithium rechargeable batteries by compounding LiTFSI, PVDF-HFP and LLZTO

Yuanchun Gu^{1,*}, Faqian Liu², Guangye Liu¹

¹ Engineering Research Center of High Performance Polymer and Molding Technology, Ministry of Education, Qingdao University of Science and Technology, Qingdao 266042, China.

² School of Chemical Engineering and Technology, Sun Yat-sen University, Zhuhai 519082, China.

*E-mail: yuanchungu@163.com

Received: 25 August 2020 / Accepted: 9 October 2020 / Published: 31 October 2020

The addition of $\text{Li}_7\text{La}_3\text{Zr}_{1.4}\text{Ta}_{0.6}\text{O}_{12}$ (LLZTO) particles to polymer electrolytes can reduce the crystallinity of polymer materials, promote the migration of lithium ions, and then improve the ionic conductivity of polymer solid electrolytes. Oxide-polymer composite solid electrolytes with different contents of LLZTO were prepared from Lithium bis(trifluoromethylsulphonyl)imide (LiTFSI), polyvinylidene fluoride-hexafluoropropylene (PVDF-HFP) and LLZTO powder as raw materials. The study has found that the solid electrolyte with 15 wt% LLZTO has higher ionic conductivity and mechanical strength, and has a wider electrochemical window (5.5V). The prepared composite cathode electrode/solid electrolyte/composite anode electrode solid-state lithium ion battery has a charge-discharge specific capacity of 179.56 mAh/g and 146.73 mAh/g for the first cycle, the coulombic efficiency is of 84%, and the discharge capacity retention rate after 30 cycles is above 94%. In addition, the change of impedance before and after the cycle is small, showing good interface stability.

Keywords: Solid-state lithium battery, Composite solid electrolyte, LLZTO, LiTFSI, PVDF-HFP

1. INTRODUCTION

All-solid-state lithium-ion batteries use non-flammable inorganic solid-state electrolytes instead of organic electrolytes used in commercial lithium-ion batteries, which can solve the safety problems of lithium-ion batteries. The solid electrolyte has good thermal and chemical stability, and there are fewer side reactions between the solid electrolyte and the electrode in the process of charge and discharge, which makes the cycle and storage life of the battery longer [1]. Therefore, solid lithium battery is expected to be the next generation lithium battery which can be used in the field of energy

storage such as electric vehicles, and has become a research hotspot in the field of energy storage [2-5].

In recent years, research on all-solid-state lithium-ion batteries has focused on developing all-solid electrolytes with high ionic conductivity, and solving the problem of high impedance between the solid electrolyte membrane and the anode interface of the battery. Common solid electrolytes include polymer-based solid electrolytes, inorganic solid electrolytes and organic-inorganic composite solid electrolytes [6]. Solid polymer electrolytes are mostly studied in solid polyoxyethylene (PEO)-based electrolytes. The solid-state electrolyte composed of PEO-based lithium-ion battery has the advantages of good shape controllability, good safety and good contact wettability with electrode materials. However, PEO is easy to crystallize at room temperature, and the solubility of Lithium Salt in PEO is low, which results in low carrier concentration. The ionic conductivity at room temperature is only 10^{-7} S/cm, and the electrochemical window of polymer solid electrolyte is narrow [7-9]. The common inorganic solid electrolytes are sulfide solid electrolyte and oxide solid electrolyte. The ionic conductivity of sulphide solid electrolyte is in the range of 10^{-4} ~ 10^{-3} S/cm, which has good formability and low softening temperature, but the material is very sensitive to moisture in the atmosphere, which brings a lot of difficulties to practical application [10-12]. The ionic conductivity of the solid electrolyte with NASICON structure $\text{Li}_{1+x}\text{Al}_x\text{Ti}_{2-x}(\text{PO}_4)_3$ (LATP) is of 10^{-4} S/cm, but the structure of the material is complex, the sintering property is poor, and the density of the sample is low. The oxide solid electrolyte $\text{Li}_{3x}\text{La}_{2/3-x}\text{TiO}_3$ (LLTO) with perovskite structure has stable structure, simple preparation process and wide range of variable composition, but its ionic conductivity at room temperature is only of 10^{-5} S/cm [13-15]. The $\text{Li}_7\text{La}_3\text{Zr}_2\text{O}_{12}$ (LLZO) with garnet structure has two kinds of structures: cubic phase and tetragonal phase. The ionic conductivity of cubic phase LLZO can reach 3×10^{-4} S/cm at room temperature, and the ionic conductivity of LLZTO obtained by tantalum doping can reach more than 10^{-3} S/cm. It is an excellent solid electrolyte material [16-19]. However, the solid-state lithium-ion battery composed of oxide solid electrolyte has high interface impedance and poor rate charge and discharge performance [20-23].

The organic-inorganic composite solid electrolytes prepared by the fusion of lithium salts, polymer electrolytes and ceramic powders with high ionic conductivity can effectively solve the problems of the above two kinds of solid electrolytes [24-26]. In order to improve the ionic conductivity of polymer solid electrolytes, inorganic ceramic fillers such as SiO_2 [27-29], Al_2O_3 [30-33] and TiO_2 [34-35] are usually added to the polymer system. These ceramic powders promote the migration of lithium ions in the polymer by reducing the crystallinity of the polymer, and then improve the ionic conductivity of the electrolyte. However, inorganic filler powders are insulating materials and do not have ionic conductivity. If superionic conductors are used as inorganic fillers, it should be more effective to improve the ionic conductivity of composite electrolytes. Garnet ceramic powder is stable for lithium metal and has a wide electrochemical working window, and especially the room temperature conductivity of Ta doped $\text{Li}_{6.4}\text{La}_3\text{Zr}_{1.4}\text{Ta}_{0.6}\text{O}_{12}$ (LLZTO) is more than 10^{-3} S/cm [36-37]. The inorganic-organic composite electrolyte membrane is easy to connect with the traditional lithium-ion battery process, has good mechanical strength and processability, and is suitable for large-scale production. The solid-state electrolyte skillfully combines the advantages of inorganic solid-state electrolyte and polymer solid-state electrolyte, can prepare all-solid-state batteries with good cycle

stability, good rate performance and strong mechanical properties, and can meet the preparation needs of large-size and high-performance batteries. It accords with the development direction of all-solid-state lithium-ion battery with safety, high specific energy and high efficiency in the future.

In this paper, composite solid electrolyte membranes with different LLZTO contents were prepared by compounding LLZTO, LiTFSI and PVDF-HFP. The introduction of LLZTO powder can effectively reduce the crystallinity of the polymer matrix, introduce a large number of new channels of Li⁺ migration, increase the electrical conductivity of the electrolyte membranes, and enhance the mechanical properties of the electrolyte membrane. The solid-state lithium-ion battery composed of LiNi_{0.6}Co_{0.2}Mn_{0.2}O₂ (NCM622) composite cathode, graphite composite anode and composite solid electrolyte membrane has good cycle performance, rate performance and interface stability.

2. EXPERIMENTAL

2.1 Preparation of electrolyte membrane and composite electrode

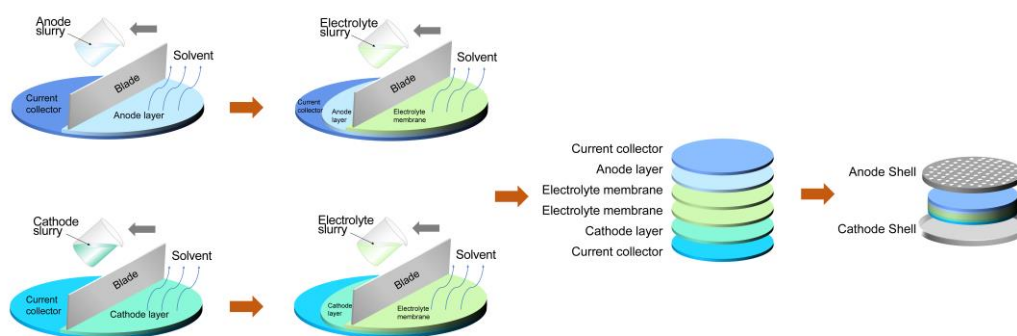
The raw materials PVDF-HFP, Li (CF₃SO₂)₂N (LiTFSI) and LLZTO powder were vacuum dried at 60 °C for 12 h. According to the mass ratio (LiTFSI : PVDF-HFP) = 6 : 4, weigh these materials, and add 0 wt%, 10 wt%, 15 wt%, and 20 wt% LLZTO powder respectively, labeled as 0% LLZTO/PVDF-HFP, 10% LLZTO/PVDF-HFP, 15% LLZTO/PVDF-HFP, and 20% LLZTO/PVDF-HFP. Add the material to an appropriate amount of N,N-dimethylformamide(DMF) solution (solid content is controlled at 30%), mechanically stir for 3 h until uniformly dispersed, and let it stand for 1 h under vacuum to remove bubbles in the slurry. Use a small casting machine to uniformly coat the surface of the PET film, dry in a vacuum drying oven at 60 °C for 2 h, dry in a blast drying oven at 50 °C for 3 h, and finally vacuum dry for 6 h to obtain a composite solid electrolyte membrane.

The composite cathode paste was obtained by adding fully dried 83 wt% NCM622, 5 wt% PVDF-HFP, 1 wt% CNTs, 2 wt% Super P, 5 wt% LLZTO and 4 wt% LiTFSI to the appropriate amount of 1-methyl-2 pyrrolidone(NMP) solvent and mechanically stirring for 2 h until it was uniformly dispersed. Stand in vacuum for 1 h to remove bubbles from the slurry. Then, the slurry was uniformly coated on the carbon-coated aluminum foil, and the composite cathode sheet was obtained after blast drying at 90 °C for 30 min and vacuum drying at 85 °C for 12 h. 78 wt% graphite, 5 wt% PVDF-HFP, 2 wt% Super P, 5 wt% LLZTO and 10 wt% LiTFSI were similarly used in the preparation of composite anodes, and the preparation method was the same as that of composite cathodes.

2.2 Assembly of CR2032 cell

The composite solid electrolyte slurry was coated on the surface of the composite cathode and composite anode respectively, and the composite cathode and composite anode were obtained by vacuum drying at 65 °C for 0.5 h and blast drying at 50 °C for 4 h. Finally, the composite cathode and composite anode were obtained after vacuum drying for 6 h. As shown in the process flow chart Scheme. 1, in the operation box, the two sides coated with electrolyte were bonded and cold pressed at

25 °C and 0.2 MPa for 1 min to make it in close contact and reduce its interface impedance. Finally, a complete CR2032 solid-state lithium-ion cell was obtained.



Scheme 1. Schematic illustrations of the preparation process for composite solid electrolyte and CR2032 cell

2.3 Structural characterization and Electrochemical testing of Materials

The surface morphology of the product was observed by scanning electron microscope (SEM, Hitachi SMI 3400N) under 5KV voltage. The phase structure of the organic-inorganic composite solid electrolyte membrane was characterized by Bruker D8 Advance X-ray diffractometer, and the mechanical properties of the electrolyte membrane were tested by ZQ-990A tension tester. The cell was assembled in a glove box filled with Ar gas (H_2O , $O_2 < 0.1$ ppm, Braun Unilab, USA). The charge-discharge (GCD) tests were carried out at different constant current densities on the Land CT2001A circulator. Cyclic voltammetry (CV) and electrochemical impedance spectroscopy (EIS) were performed by GAMRY Reference3000 electrochemical workstation.

3. RESULTS AND DISCUSSION

3.1 The analysis of solid electrolyte membranes with different LLZTO content

Fig. 1 (a) shows the X-ray diffraction patterns of solid electrolyte membranes with different LLZTO contents. The electrolyte membranes containing LLZTO coincides with the standard card PDF#45-0109 and meets the special crystal structure characteristics of cubic garnet. With the increase of LLZTO content, the peak intensity increases gradually, and there is no obvious hetero-peak, which indicates that there is no obvious change in crystal structure when LLZTO is compounded with PVDF-HFP and lithium salt. No obvious characteristic peak of lithium salt (LiTFSI) is found in the XRD spectrum, indicating that lithium salt can be well compounded with PVDF-HFP matrix. Fig. 1(b) is a surface SEM photograph of a solid electrolyte membrane containing 15 wt% LLZTO. It can be seen from the figure that the particle size of LLZTO is uniform and the distribution is uniform. Under the

action of binder PVDF-HFP, the electrolyte membrane is uniform and compact, and the membrane-forming property is good. At the same time, it can be seen that the small lithium salt particles are uniformly attached to the LLZTO. This distribution structure can increase the ionic conductivity of the solid electrolyte membrane and reduce the interface impedance of the solid electrolyte membrane.

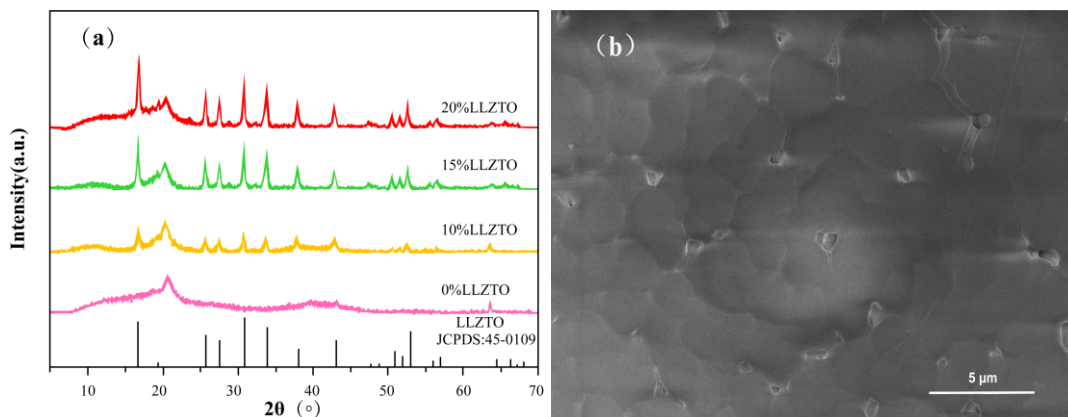


Figure 1. (a) XRD patterns and (b) surface SEM image of organic-inorganic composite solid electrolyte.

3.2 The effect of LLZTO content on the ionic conductivity of composite solid electrolyte membrane at different temperature

Fig. 2 (a) shows the relationship between the ionic conductivity of solid electrolyte membranes with different LLZTO content and ambient temperature at -10 °C to 80 °C. The AC impedance of solid electrolyte membranes with different LLZTO content is measured by electrochemical workstation at the temperature of -10 ~ 80 °C. Fig. 2 (b) shows the AC impedance spectrum at 30 °C. After obtaining the AC impedance spectrum, the appropriate fitting circuit is selected to fit the impedance of different solid-state electrolyte membranes by Zview software, and the resistance of solid-state electrolyte membranes is obtained. The ionic conductivity of solid electrolyte membranes with different LLZTO content is calculated by using the following equation.

$$\sigma = \frac{1}{R} \times \frac{d}{A}$$

While (R) is denoted as the impedance of the solid electrolyte membrane, (d) is the thickness of the membrane, and (A) represents the area of the electrolyte sample. It can be seen from Fig. 2 (a) that the ionic conductivity of solid electrolyte membranes increases with the increase of temperature. At the same temperature, the ionic conductivity of solid electrolyte membranes with different LLZTO content is in the following order: 15 wt% LLZTO > 20 wt% LLZTO > 10 wt% LLZTO > 0 wt% LLZTO. As a good lithium ion conductor, the ionic conductivity of LLZTO can reach 10^{-4} S/cm, which is much higher than that of the mixed electrolyte of PVDF-HFP and LiTFSI. Therefore, with the increase of LLZTO content, a large number of new channels of Li⁺ migration are introduced into the solid electrolyte, which increases the ionic conductivity of the electrolyte membrane. However, with the increase of LLZTO content, the ionic conductivity of solid electrolyte membrane containing 20 wt%

LLZTO decreases. This may be due to the fact that with the increase of LLZTO content, excessive LLZTO particles adhere to the pore wall of the micropores in the electrolyte membrane, blocking the migration channel of Li⁺, thus reducing the ionic conductivity of the electrolyte membrane. Therefore, when the solid electrolyte membrane contains 20 wt% LLZTO, the ionic conductivity of the solid electrolyte membrane is significantly lower than that of the electrolyte membrane containing 15 wt% LLZTO. Fig. 2 (c) shows the stress-strain curves of solid electrolyte membranes with different LLZTO contents. It can be seen from the figure that with the increase of LLZTO content, the tensile strength and Young's modulus of the solid electrolyte membrane increase obviously, and the elongation of the membrane decreases, which is due to the adhesion effect between PVDF-HFP polymer matrix and LLZTO particles. Fig. 2 (d) shows the linear scanning voltammetry curve of solid electrolyte membrane. The scanning voltage range is 2.5 ~ 6.0V, and the scanning speed is 0.1 V/s. It can be seen from the Fig. 2 (d) that the solid electrolyte containing 15 wt% LLZTO has a wider electrochemical window (5.5 V), indicating that the addition of LLZTO can improve the electrochemical stability of solid electrolyte.

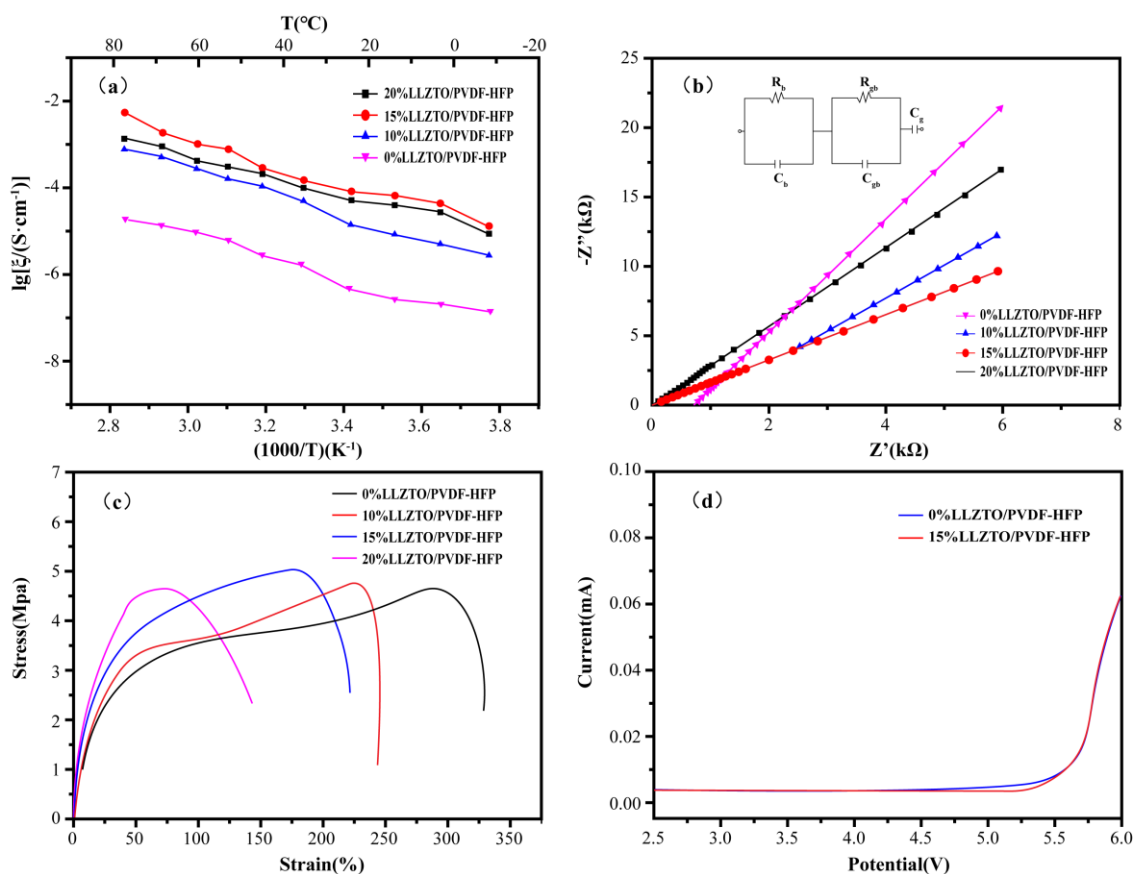


Figure 2. Solid electrolyte membranes with different LLZTO contents; (a) ionic conductivity versus temperature; (b) AC impedance spectra at 30°C; (c) stress-strain curves; (d) linear sweep voltammetry curves.

3.3 Research on battery electrochemical performance

Fig. 3 (a) shows the cycle performance of NCM622 composite cathode/organic-inorganic composite solid electrolyte/graphite composite anode. At room temperature, the charge and discharge rate is 0.05 C and the battery is cycled for 30 times. The first charge-discharge specific capacity of the battery is 179.56 and 146.73 mAh/g respectively, and the first Coulomb efficiency is 84%. After 30 cycles, the Coulomb efficiency of the battery can be maintained above 96%. Fig. 3 (b) shows the discharge capacity retention of the battery. At room temperature, the discharge capacity can reach 94% of the initial discharge capacity after 30 cycles, which shows that the battery has less polarization during the cycle and has good cycle performance. At 25 °C, the voltage range is 3 to 4.2 V. When the battery is discharged at a rate of 0.05 C, the voltage platform is about 3.6 V, and the discharge specific capacity of the battery is 145.3 mAh/g. The discharge specific capacity of the battery is 139.69, 129.47 and 104.85 mAh/g at 0.1 C, 0.2 C, and 0.5 C respectively. Fig. 3 (d) shows the rate performance of solid-state battery. It can be seen that the discharge specific capacity of the battery decreases with the increase of discharge rate, which may be caused by the increase of internal polarization of the battery. In the process of high-rate charge and discharge, the intercalation and de-intercalation process of Li⁺ is not complete, which also leads to the decline of battery capacity.

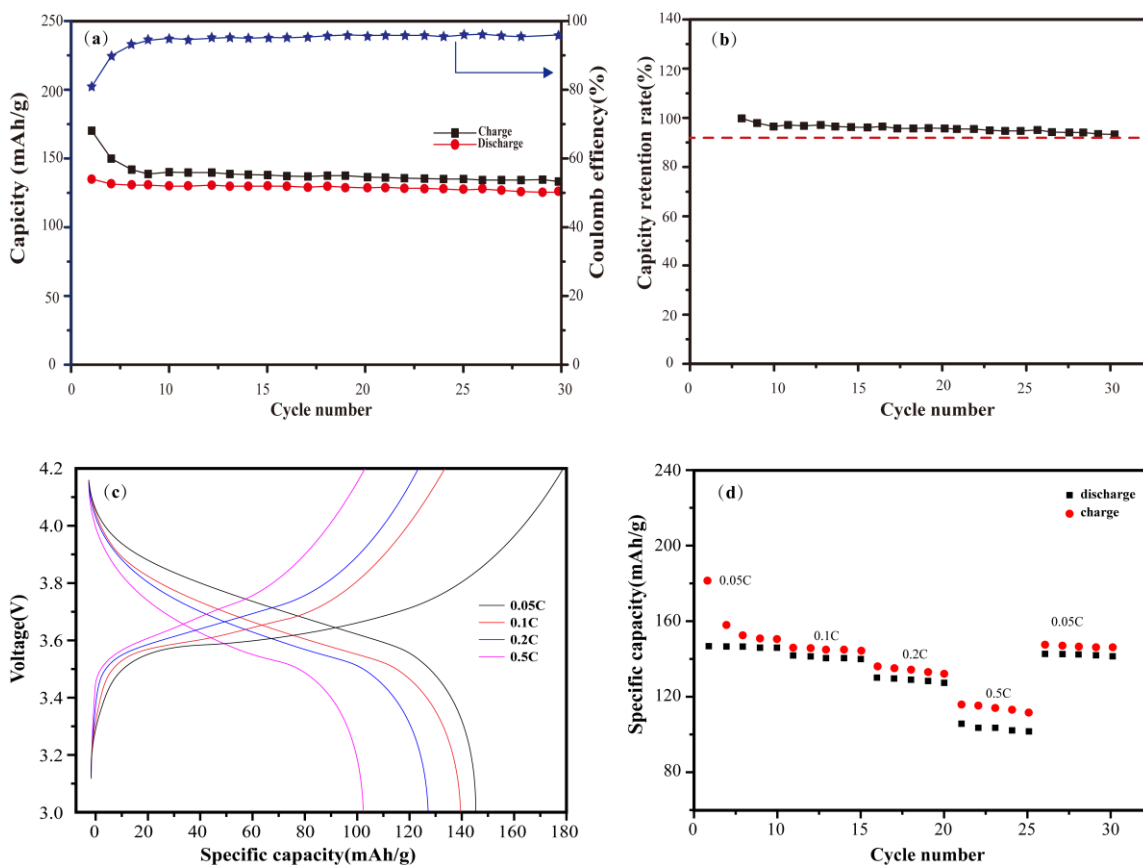


Figure 3. NCM622 composite cathode electrode/organic-inorganic composite solid electrolyte/graphite composite anode solid state battery at 25°C; (a) cycle performance curve; (b) discharge capacity decay rate; (c) rate charge-discharge curve; (d) rate performance curve.

Fig. 4 shows the AC impedance spectrum of the all-solid-state lithium-ion battery composed of NCM622 composite cathode/organic-inorganic composite solid electrolyte/graphite composite anode before and after 30 cycles at 25 °C. It can be seen from Fig. 4 that the impedance of the all-solid-state lithium-ion battery before circulation is about 6 Ω, and the internal resistance of the battery increases to 14 Ω after 30 cycles. The change in battery impedance before and after the solid-state battery cycle is small, indicating that the solid-state battery of this structure has lower interface impedance and good interface compatibility, and the chemical stability of the internal electrode interface of the battery is better.

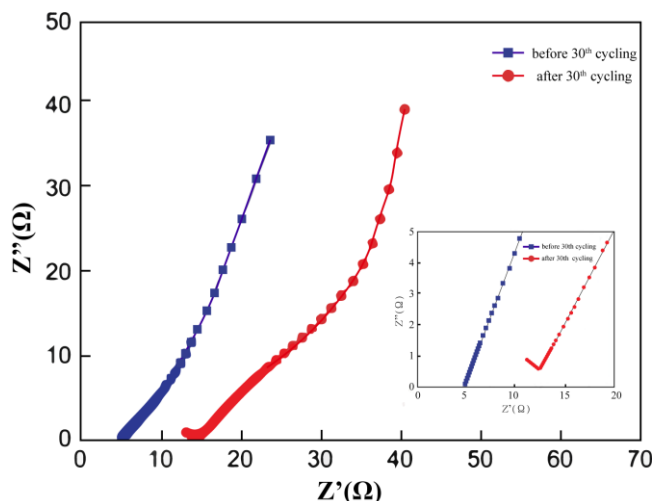


Figure 4. AC impedance spectrum before and after cycling at 25°C for solid state battery with NCM622 composite cathode/organic-inorganic composite solid electrolyte/graphite composite anode.

Table 1. Comparison of battery performance of the cell with previously reported ASSBs

Electrolyte	Ion-conductivity/ (mS.cm ⁻¹)	Cathode material	Interface Engineering	Test condition	Discharge capacity/ (mAh.g ⁻¹)	Ref
Li ₇ La ₃ Zr _{1.4} Ta _{0.6} O ₁₂	2.26	LiFePO ₄	Coating	25 °C 3-4.2 V	146(1 st) 137(30 th)	
Li _{6.20} Ga _{0.30} La _{2.95} Rb _{0.05} Zr ₂ O ₂	1.62	LiFePO ₄	Coating	60 °C 5 μA.cm ⁻² 2.8-4.0 V	152(1 st) 110(20 th)	[38]
Li _{6.4} La ₃ Zr _{1.4} Ta _{0.6} O ₁₂	1.60	LiFePO ₄	Coating	60°C 0.05C 2.76-4.0 V	150(1 st) 140(100 th)	[36]
Li ₇ La ₃ Zr ₂ O ₁₂	2.40	LiFePO ₄	Coating	25 °C 0.1 C	160.4(1 st) 136.8(100 th)	[39]
Li _{6.75} La ₃ Zr _{1.75} Ta _{0.25} O ₁₂	1.00	LiCoO ₂	Coating+	5 μA.cm ⁻²	101.3(1 st)	[40]
Li _{6.75} La ₃ Zr _{1.75} Ta _{0.25} O ₁₂	0.74	LiNi _{0.5} Co _{0.2} Mn _{0.3} O ₁₂	Co-sintering Tape casting	80 °C 5 μA.cm ⁻² 3.0-4.6 V	123.3(1 st) 76.6(5 th)	[41]
Li _{6.25} Al _{0.25} La ₃ Zr ₂ O ₁₂	0.50	Li ₄ Ti ₅ O ₁₂	Coating	95 °C 2-8 μA.g ⁻¹ 1.0-2.5 V	15(1 st)	[42]

The composite electrolyte membrane composed of PVDF matrix and Li_{6.75}La₃Zr_{1.75}Ta_{0.25}O₁₂ shows excellent electrochemical performance, mechanical properties and good thermal stability at

ambient temperature, and can effectively improve the interface structure and interface contact performance between cathode and electrolyte [43]. Compared with PVDF, PVDF-HFP has functional groups with electron adsorption effect and low crystallinity, showing higher electrical conductivity. c.w SUN of Beijing Institute of Nano Energy and Systems, Chinese Academy of Sciences, compounded $\text{Li}_7\text{La}_3\text{Zr}_2\text{O}_{12}$ with PVDF-HFP, and the composite electrolyte membrane and cathode material also had good interface contact properties and low solid/solid interface impedance, and could be wound and bent, showing excellent mechanical properties [44]. Tab. 1 shows the comparison of the electrochemical performance of the battery prepared in this paper with that of the previously reported all solid state battery (ASSB). It can be seen that although the preparation methods are different and the test conditions are different, the battery prepared in this paper still has advantages in ionic conductivity and charge-discharge performance.

4. CONCLUSIONS

In this paper, organic-inorganic composite solid electrolyte membranes with different LLZTO contents and an all-solid-state lithium ion battery with a composite cathode/solid electrolyte/graphite composite anode structure were prepared. The study has found that the ionic conductivity of the solid electrolyte membrane increases with increasing temperature, and under the same temperature conditions, as the content of LLZTO increases, the ionic conductivity of the electrolyte membrane increases first and then decreases. The electrolyte membrane containing 15 wt% LLZTO has the highest ion conductivity, indicating that the introduction of a suitable amount of fast ion conductor can improve the ion conductivity of the electrolyte membrane, but excessive addition is not conducive to the improvement of electrolyte ion conductivity. The solid electrolyte containing 15 wt% LLZTO has better mechanical properties and a wider electrochemical window than the undoped LLZTO solid electrolyte, indicating that the addition of LLZTO can improve the tensile strength, Young's modulus and electrochemistry of the solid electrolyte stability. The initial charge-discharge specific capacity of the prepared composite cathode/solid electrolyte/composite anode all-solid-state lithium-ion battery is 179.56 and 146.73 mAh/g respectively. After 30 cycles, the Coulomb efficiency can be maintained above 96%, and the discharge capacity retention rate of the cell is more than 94%. The change of interface impedance before and after cycling is small, and the cell shows good cyclicality, rate performance and good interface stability.

References

1. P. Verma, P. Maire, and P. Novák, *Electrochim. Acta*, 55 (2010) 6332.
2. H. Li, M. Li, S. H. Siyal, M. Zhu, J.-L. Lan, G. Sui, Y. Yu, W. Zhong, and X. Yang, *J. Membr. Sci.*, 555 (2018) 169.
3. X. Ban, W. Zhang, N. Chen, and C. Sun, *The Journal of Physical Chemistry C*, 122 (2018) 9852.
4. S. Yu, S. Schmohl, Z. Liu, M. Hoffmeyer, N. Schön, F. Hausen, H. Tempel, H. Kungl, H. D. Wiemhöfer, and R. A. Eichel, *Journal of Materials Chemistry A*, 7 (2019) 3882.

5. L. Fan, S. Wei, S. Li, Q. Li, and Y. Lu, *Advanced Energy Materials*, 8 (2018) 1702657.
6. Z. Qiu, Y. Zhang, S. Xia, and P. Dong, *Acta Chimica Sinica*, 73 (2015) 992.
7. K. Takada, *J. Power Sources*, 394 (2018) 74.
8. W. Gorecki, M. Jeannin, E. Belorizky, C. Roux, and M. Armand, *J. Phys.: Condens. Matter*, 7 (1995) 6823.
9. E. Cznotka, S. Jeschke, M. Grünebaum, and H.-D. Wiemhöfer, *Solid State Ionics*, 292 (2016) 45.
10. N. Kamaya, K. Homma, Y. Yamakawa, M. Hirayama, R. Kanno, M. Yonemura, T. Kamiyama, Y. Kato, S. Hama, and K. Kawamoto, *Nat. Mater.*, 10 (2011) 682.
11. Y. Kato, S. Hori, T. Saito, K. Suzuki, M. Hirayama, A. Mitsui, M. Yonemura, H. Iba, and R. Kanno, *Nature Energy*, 1 (2016) 1.
12. Y. Deng, C. Eames, J.-N. L. Chotard, F. Lalère, V. Seznec, S. Emge, O. Pecher, C. P. Grey, C. Masquelier, and M. S. Islam, *J. Am. Chem. Soc.*, 137 (2015) 9136.
13. Z. Deng, B. Radhakrishnan, and S. P. Ong, *Chem. Mater.*, 27 (2015) 3749.
14. G. Y. Adachi, N. Imanaka, and H. Aono, *Adv. Mater.*, 8 (1996) 127.
15. X. Wang, Y. Zhang, X. Zhang, T. Liu, Y.-H. Lin, L. Li, Y. Shen, and C.-W. Nan, *ACS Appl. Mater. Interfaces*, 10 (2018) 24791.
16. J. B. Goodenough, and P. Singh, *J. Electrochem. Soc.*, 162 (2015) A2387.
17. Y. Li, Z. Wang, Y. Cao, F. Du, C. Chen, Z. Cui, and X. Guo, *Electrochim. Acta*, 180 (2015) 37.
18. R.-J. Chen, M. Huang, W.-Z. Huang, Y. Shen, Y.-H. Lin, and C.-W. Nan, *Solid State Ionics*, 265 (2014) 7.
19. M. Huang, M. Shoji, Y. Shen, C.-W. Nan, H. Munakata, and K. Kanamura, *J. Power Sources*, 261 (2014) 206.
20. M. Zhu, J. Wu, W. H. Zhong, J. Lan, G. Sui, and X. Yang, *Advanced Energy Materials*, 8 (2018) 1702561.
21. M. Li, H. Li, J.-L. Lan, Y. Yu, Z. Du, and X. Yang, *Journal of Materials Chemistry A*, 6 (2018) 19094.
22. Y. Shen, Y. Zhang, S. Han, J. Wang, Z. Peng, and L. Chen, *Joule*, 2 (2018) 1674.
23. J. Zhang, X. Zang, H. Wen, T. Dong, J. Chai, Y. Li, B. Chen, J. Zhao, S. Dong, and J. Ma, *Journal of Materials Chemistry A*, 5 (2017) 4940.
24. C. W. Walker Jr, and M. Salomon, *J. Electrochem. Soc.*, 140 (1993) 3409.
25. C. Angell, K. Xu, S. Zhang, and M. Videa, *Solid State Ionics*, 86 (1996) 17.
26. J. W. Fergus, *J. Power Sources*, 195 (2010) 4554.
27. S. Ketabi, and K. Lian, *Electrochim. Acta*, 103 (2013) 174.
28. L. Fan, C.-W. Nan, and S. Zhao, *Solid State Ionics*, 164 (2003) 81.
29. J.-W. Kim, K.-S. Ji, J.-P. Lee, and J.-W. Park, *J. Power Sources*, 119 (2003) 415.
30. S. K. Fullerton-Shirey, and J. K. Maranas, *The Journal of Physical Chemistry C*, 114 (2010) 9196.
31. M. R. Johan, O. H. Shy, S. Ibrahim, S. M. M. Yassin, and T. Y. Hui, *Solid State Ionics*, 196 (2011) 41.
32. Q. Li, Y. Takeda, N. Imanish, J. Yang, H. Sun, and O. Yamamoto, *J. Power Sources*, 97 (2001) 795.
33. H. Pitawala, M. Dissanayake, and V. Seneviratne, *Solid State Ionics*, 178 (2007) 885.
34. K. Vignarooban, M. Dissanayake, I. Albinsson, and B.-E. Mellander, *Solid State Ionics*, 266 (2014) 25.
35. S. Ketabi, and K. Lian, *Electrochim. Acta*, 154 (2015) 404.
36. F. Du, N. Zhao, Y. Li, C. Chen, Z. Liu, and X. Guo, *J. Power Sources*, 300 (2015) 24.
37. Y. Jin, K. Liu, J. Lang, D. Zhuo, Z. Huang, C.-A. Wang, H. Wu, and Y. Cui, *Nature energy*, 3 (2018) 732.
38. J.-F. Wu, W. K. Pang, V. K. Peterson, L. Wei, and X. Guo, *ACS Appl. Mater. Interfaces*, 9 (2017) 12461.
39. X. Yan, Z. Li, Z. Wen, and W. Han, *The Journal of Physical Chemistry C*, 121 (2017) 1431.
40. T. Liu, Y. Ren, Y. Shen, S.-X. Zhao, Y. Lin, and C.-W. Nan, *J. Power Sources*, 324 (2016) 349.

41. T. Liu, Y. Zhang, X. Zhang, L. Wang, S.-X. Zhao, Y.-H. Lin, Y. Shen, J. Luo, L. Li, and C.-W. Nan, *Journal of Materials Chemistry A*, 6 (2018) 4649.
42. J. Van Den Broek, S. Afyon, and J. L. Rupp, *Advanced Energy Materials*, 6 (2016) 1600736.
43. X. Zhang, T. Liu, S. Zhang, X. Huang, B. Xu, Y. Lin, B. Xu, L. Li, C.-W. Nan, and Y. Shen, *J. Am. Chem. Soc.*, 139 (2017) 13779.
44. W. Zhang, J. Nie, F. Li, Z. L. Wang, and C. Sun, *Nano Energy*, 45 (2018) 413.

© 2020 The Authors. Published by ESG (www.electrochemsci.org). This article is an open access article distributed under the terms and conditions of the Creative Commons Attribution license (<http://creativecommons.org/licenses/by/4.0/>).